Limitations of Using Passivity Index to Analyze Grid–Inverter Interactions

Feifan Chen, *Graduate Student Member, IEEE*, Xiongfei Wang, *Fellow, IEEE*, Lennart Harnefors, *Fellow, IEEE*, Sei Zhen Khong, Dan Wang, *Member, IEEE*, Liang Zhao, *Member, IEEE*, Kin Cheong Sou, *Member, IEEE*, Mikko Routimo, *Member, IEEE*, Jarno Kukkola, Henrik Sandberg, *Fellow, IEEE*, and Karl Henrik Johansson, *Fellow, IEEE*

***Abstract*—The main purpose of this article is to elaborate on the limitations of using frequency-domain passivity theories in analyzing grid-inverter interactions within the low-frequency range. It primarily covers three levels of limitations: 1) the limitations and selection criteria of two kinds of passivity index, 2) potential conflicts between different passivity index tuning methods, and 3) the relationship between the frequency range of negative passivity index and system stability robustness. The findings suggest that caution should be exercised when applying passivity theory, particularly in the low-frequency range.**

***Index Terms*—Control design, grid-connected inverters, passivity, stability.**

I. Introduction

GRID-CONNECTED inverters are commonly found in modern power systems. An effective design of control parameters for such inverters is critical for ensuring the stability of the system [1]. The conventional methods of evaluating system stability, such as eigenvalue-based or Nyquist criteria-based analysis, require aggregating information from both the inverter and the grid [2]. However, in a system with multiple inverters, this aggregation of information is complex and computationally burdensome [3]. Moreover, it is often not possible to obtain detailed information on the grid. Passivity theory offers a valuable decentralized perspective to system analysis [4]. The basic idea is that if a system is composed of passive subsystems, then the system is stable regardless of the complexity of the interactions among the subsystems [5]. When applying passivity theory to analyze grid-connected inverter systems, it is not necessary to know the detailed parameters of the grid side, assuming it is passive [6]. The aggregation of information from the inverter and the grid is also not required [7]. By properly designing parameters [8] or adding additional controllers [9], the input admittance of the inverter can have a positive real part in the critical frequency ranges where poorly damped grid resonances appear [10]. Thereby, destabilization of such resonances can be avoided [7].

Passivity-based analysis can be categorized into high-frequency and low-frequency cases [11]. In the high-frequency scenario, the focus is on harmonic instability, usually in the range of several hundred to several thousand hertz [4], [12]. In this frequency range, system instability usually originates from the impedance characteristics of the grid itself, the time delay due to digital computation and pulsewidth modulation of inverters [11]. Slower outer loop control dynamics, such as power control (PC), phase-locked loop (PLL), and alternating-voltage control (AVC) are often ignored [1]. Numerous studies have focused on the passivation or dissipation of grid-connected inverters, including parameter tuning [4], improved sampling techniques [12], and control design [13].

In the low-frequency range, the focus is on near-synchronous oscillations, which are usually no more than three times the nominal frequency [6]. In this range, asymmetric and slow dynamics of outer loops can no longer be ignored [14]. Therefore, the inverter needs to be modeled as a multiple-input multiple-output (MIMO) system [1]. Two kinds of *passivity index*, namely, the input feedforward passivity (IFP) index and output feedback passivity (OFP) index are commonly used to analyze the MIMO systems [15], [16]. In [3], [11], for example, it is demonstrated that grid-connected inverters have inherently nondissipative low-frequency regions that are difficult to avoid. As a result, the passivity-based design usually recommends minimizing nondissipative regions [6] or increasing the value of the passivity index [16] to enhance system stability robustness. However, there are gray areas in passivity theory when it comes to guiding the design or assessing the stability of such MIMO dynamical systems. First, the distinction between the IFP index and the OFP index, the criteria for selecting different indices, and the varying stability criteria based on these indices are all unclear. Second, there is a lack of discussion on the selection, comparison, and

Manuscript received 5 February 2024; revised 29 June 2024; accepted 10 July 2024. Date of publication 15 July 2024; date of current version 11 September 2024. The work of Sei Zhen Khong was supported by the National Science and Technology Council of Taiwan under Grant 113-2222-E-110-002-MY3. Recommended for publication by Associate Editor Marta Molinas. *(Corresponding author: Xiongfei Wang.)*

Feifan Chen, Xiongfei Wang, Dan Wang, Liang Zhao, Henrik Sandberg, and Karl Henrik Johansson are with the School of Electrical Engineering and Computer Science, KTH Royal Institute of Technology, 10044 Stockholm, Sweden (e-mail: feifanc@kth.se; xiongfei@kth.se; danwang@kth.se; liazhao@kth.se; hsan@kth.se; kallej@kth.se).

Lennart Harnefors is with ABB Corporate Research, 72226 Västeras, Sweden (e-mail: lennart.harnefors@se.abb.com).

Sei Zhen Khong and Kin Cheong Sou are with the Department of Electrical Engineering, National Sun Yat-sen University, Kaohsiung City 804, Taiwan (e-mail: szkhong@mail.nsysu.edu.tw; sou12@mail.nsysu.edu.tw).

Mikko Routimo and Jarno Kukkola are with ABB Oy Drives, 00380 Helsinki, Finland (e-mail: mikko.routimo@fi.abb.com; jarno.kukkola1@fi.abb.com).

Color versions of one or more figures in this article are available at https://doi.org/10.1109/TPEL.2024.3428403.

Digital Object Identifier 10.1109/TPEL.2024.3428403

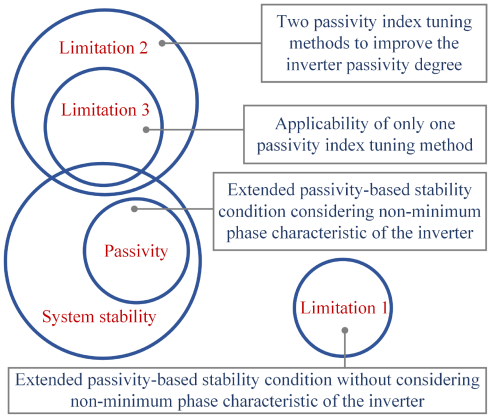

Fig. 1. Venn diagram of the relationships among stability of the system, stability conditions based on passivity theory, and the limitations of passivity theory in the low-frequency range.

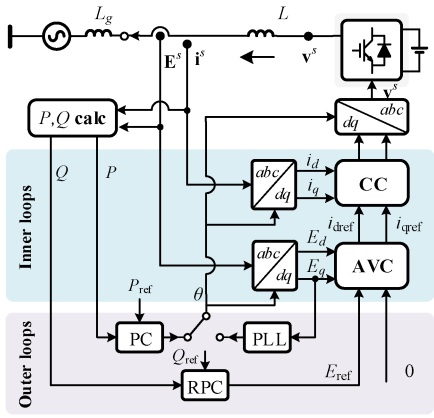

Fig. 2. System configuration and block diagram of a grid-connected inverter.

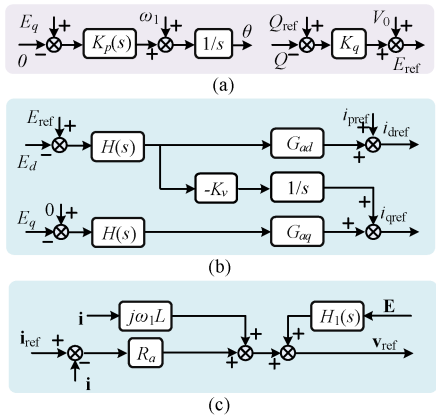

Fig. 3. Controller structure of PLL-synchronized inverter. (a) PLL and Q-V droop. (b) AVC. (c) CC.

solidness of two common passivity index tuning methods at low frequencies.

This article explores and clarifies the gray areas of frequency-domain passivity theory when applied to grid-inverter interaction analysis. The contributions lie in the discussion of the limitations of passivity theory at three levels. The first-level limitation (limitation 1) discusses the distinction between the IFP and OFP indices. The differences and connections between the indices across different system representations (current source or voltage source) are clarified. Two different stability conditions based on passivity indices are then introduced. Finally, the criteria for selecting the passivity index in grid-connected inverter systems are specified, and the consequences of incorrect index selection, which inevitably lead to system instability, are theoretically demonstrated. Specifically, the IFP index is considered a more suitable choice for the inverter admittance. The second-level limitation (limitation 2) lies in the selection of two commonly used passivity index tuning methods: reducing the frequency range of negative index values or increasing the minimum value of the passivity index. The relationship between these methods and system stability is discussed in depth both logically and through case studies. Even when the index is chosen correctly considering limitation 1, different methods of index tuning may conflict with each other and lead to inconsistent results. The third-level limitation (limitation 3) involves a deeper discussion of the relationship between reducing the frequency region of the negative index and system stability. The integrators in controllers may cause the passivity index value to approach negative infinity [17]. In such cases, the only way to tune the passivity index is to narrow the frequency region where it is negative. It is found that in this scenario, a narrower frequency range of negative index does not necessarily imply improved stability robustness, which may even cause low-frequency oscillations. Based on the findings related to limitations 2 and 3, it is not recommended to use passivity theory to analyze grid-inverter interactions in the low-frequency range, especially near $\omega = 0$ in the $d-q$ frame. The limitations discussed and contributions of this article are summarized in a Venn diagram shown in Fig. 1.

II. Grid-Connected Inverter Systems

Fig. 2 shows the overall circuit and block diagram of the grid-connected inverter system under consideration. Apart from AVC and current control (CC), there are also synchronization control and reactive power control. Currently, the mainstream synchronization control includes PLL and PC [18]. Since this article focuses on the application of the passivity theory in grid-connected inverter systems, rather than the analysis of different types of control schemes, examples from both PLL-synchronized inverters and PC-synchronized inverters are presented. The corresponding detailed structures of PC, synchronization control, voltage control, and CC are given in Figs. 3 and 4, respectively. The PLL is equipped with a P-dominant controller. The integral part aims to eliminate the quasisteady-state phase error caused by deviations in synchronous frequency from its nominal value, which can be small [5]. The P gain is α_p/E_0, where α_p represents the PLL bandwidth and E_0 denotes the steady-state voltage amplitude (equivalent to E_{ref}). The transfer functions $H(s)$, $H_1(s)$, and $H_2(s)$ model low-pass filters with bandwidth α_f. The parameter R_a is set as $\alpha_c L$, where α_c is the desired CC loop bandwidth and L is the filter inductance [5].

The impedance modeling technique of these two kinds of inverters has been extensively discussed in previous studies,

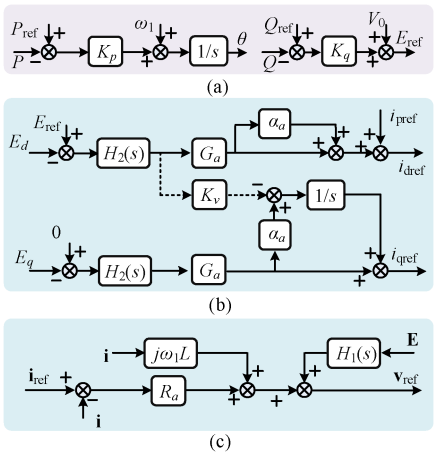

Fig. 4. Controller structure of PC-synchronized inverter. (a) P-f droop and Q-V droop. (b) AVC. (c) CC.

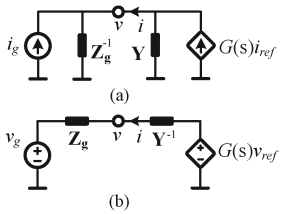

Fig. 5. System circuit representation. (a) Based on the equivalent of a current source. (b) Based on the equivalent of a voltage source.

which will not be repeated here. The modeling approach for PLL-based inverter here is consistent with the technique described in [5], [15], and [19]. The modeling of PC-synchronized inverters aligns with the approach described in [2] and [16]. The dc-link dynamics are not considered here and dc-link voltage is assumed to remain constant [20]. For the grid, it can be viewed as a voltage source in series with the grid impedance $\mathbf{Z}_g$. The grid impedance is assumed to be primarily inductive-dominated with inductance L_g, and the resistance R_g is disregarded when modeling the system for worst-case analysis, where no passive damping from the grid side is considered [16]. Regarding inverters, there are typically two circuit representation methods [21], namely the equivalent based on a current source in parallel with the admittance $\mathbf{Y}$ and the equivalent based on a voltage source in series with impedance, as shown in Fig. 5. The closed-loop transfer function of the voltage or CC is denoted by $G(s)$. To avoid potential redundancy and confusion, the impedance corresponding to the voltage source representation is represented in this article using the reciprocal of admittance $\mathbf{Y}$.

III. Preliminaries of Passivity Theory in Grid-Connected Inverter Systems

A. Definition of Passivity and Corresponding Physical Insights

For a general stable and minimum-phase MIMO system $\mathbf{G}$, $\mathbf{G}$ is said to be strictly "input feedforward passive" [22] if

$$\min \lambda \left[\mathbf{G}\left(j\omega\right)+\mathbf{G}^{H}\left(j\omega\right)\right]>0, \forall \omega \in [0,\infty] \tag{1}$$

holds and $\mathbf{G}$ is strictly "output feedback passive" [22] if

$$\min \lambda \left[\mathbf{G}^{-1}\left(j\omega\right)+\mathbf{G}^{-H}\left(j\omega\right)\right]>0, \forall \omega \in [0,\infty] \tag{2}$$

holds, where min λ is the minimum eigenvalue and the superscript H is the Hermitian operator, i.e., conjugate–transpose. The grid impedance is passive, as mentioned in Section II. Concerning the inverter, the definition of "passive" has an intuitive physical meaning as well. In Fig. 2, the positive direction of the current is defined from the inverter to the grid. Consequently, when power is positive, it implies that the inverter is injecting active power into the grid. According to Harnefors et al.'s [5] work, the power dissipation of the inverter is given as

$$-\left(1/2\right)\left(v^{H}i+i^{H}v\right) \tag{3}$$

where v and i are complex phasors for voltages and currents at the point of common coupling (PCC), respectively. If the system is modeled as a current source in parallel with the input admittance $\mathbf{Y}$, then the relationship between voltage and current at PCC is given by

$$i=-\mathbf{Y}(j\omega)v. \tag{4}$$

Then

$$-\left(v^{H}i+i^{H}v\right)=v^{H}\left[\mathbf{Y}\left(j\omega\right)+\mathbf{Y}^{H}\left(j\omega\right)\right]v. \tag{5}$$

If $\mathbf{Y}(j\omega)+\mathbf{Y}^{H}(j\omega)$ is positive definite for all ω, then

$$v^{H}\left[\mathbf{Y}\left(j\omega\right)+\mathbf{Y}^{H}\left(j\omega\right)\right]v>0, \forall \omega \in [0,\infty] \tag{6}$$

so active power is always dissipated, i.e., the system is passive. $\mathbf{Y}+\mathbf{Y}^{H}$ is positive definite if and only if

$$\min \lambda \left[\mathbf{Y}\left(j\omega\right)+\mathbf{Y}^{H}\left(j\omega\right)\right]>0, \forall \omega \in [0,\infty]. \tag{7}$$

Similarly, if the system is modeled as a voltage source in series with the input impedance $\mathbf{Y}^{-1}$, then the relationship between voltage and current is

$$v=-\mathbf{Y}^{-1}(j\omega)i. \tag{8}$$

Hence, the active power is given by

$$-\left(v^{H}i+i^{H}v\right)=i^{H}\left[\mathbf{Y}^{-1}\left(j\omega\right)+\mathbf{Y}^{-H}\left(j\omega\right)\right]i. \tag{9}$$

If $\mathbf{Y}^{-1}(j\omega)+\mathbf{Y}^{-H}(j\omega)$ is positive definite for all ω, then active power is always dissipated, i.e., the system is passive. $\mathbf{Y}^{-1}+\mathbf{Y}^{-H}$ is positive definite if and only if

$$\min \lambda \left[\mathbf{Y}^{-1}\left(j\omega\right)+\mathbf{Y}^{-H}\left(j\omega\right)\right]>0, \forall \omega \in [0,\infty]. \tag{10}$$

Equations (7) and (10) correspond to the definitions in (1) and (2).

B. Passivity-Based Stability Conditions and Their Extensions

According to [21] and [23], the circuits depicted in Fig. 5 can be transformed into a MIMO interconnected feedback system. It should be noted that the interconnected systems come in various forms, but all can reflect the same system stability [21]. If voltage is chosen as the input and current as the output, one corresponding interconnected system can be represented as [$\mathbf{Z}_g$, $\mathbf{Y}$], where $\mathbf{Z}_g$ is the forward gain, and $\mathbf{Y}$ is the feedback gain, as shown in Fig. 6(a). The other interconnected system can be represented as [$\mathbf{Y}^{-1}$, $\mathbf{Z}_g^{-1}$], which is shown in Fig. 6(b). According to Theorem 2.44 in Bao et al.'s [22] work, for a general MIMO interconnected negative-feedback system [$\mathbf{G}_1$, $\mathbf{G}_2$], as shown in Fig. 6(c), if both $\mathbf{G}_1$ and $\mathbf{G}_2$ are strictly passive,

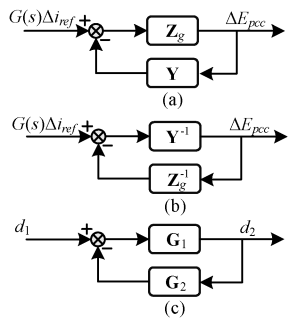

Fig. 6. Interconnected feedback system of (a) $[\mathbf{Z}_g, \mathbf{Y}]$, (b) $[\mathbf{Y}^{-1}, \mathbf{Z}_g^{-1}]$, and (c) $[\mathbf{G}_1, \mathbf{G}_2]$.

then the interconnected negative-feedback system $[\mathbf{G}_1, \mathbf{G}_2]$ is stable.

To extend the passivity-based stability conditions to more general cases that encompass both passive and nonpassive systems, passivity indices that quantify the degree of passivity are defined [22]. The basic idea is that in an interconnected system, there are both passive and nonpassive subsystems. If the excessive passivity of the passive subsystem can compensate for the passivity deficit in the nonpassive system, then the system remains stable. The passivity indices are defined in a similar manner to (1) and (2). The IFP index at frequency ω is defined as

$$\nu_F\left[\mathbf{G}(s),\omega\right] \triangleq \frac{1}{2}\min\lambda\left[\mathbf{G}\left(j\omega\right)+\mathbf{G}^H\left(j\omega\right)\right]. \tag{11}$$

Similarly, the OFP index is defined as

$$\rho_F\left[\mathbf{G}(s),\omega\right] \triangleq \frac{1}{2}\min\lambda\left[\mathbf{G}^{-1}\left(j\omega\right)+\mathbf{G}^{-H}\left(j\omega\right)\right]. \tag{12}$$

For $[\mathbf{G}_1, \mathbf{G}_2]$, here we assume that $\mathbf{G}_1$ and $\mathbf{G}_2$ are both stable and minimum phase systems (more general cases, including nonminimum phase systems, will be discussed in the next section), $\mathbf{G}_1$ is nonpassive, and $\mathbf{G}_2$ is passive. According to the definition of passivity indices, $\mathbf{G}_1$ lacks passivity (both input feedforward and output feedback), while $\mathbf{G}_2$ has an excess of passivity (the passivity index of $\mathbf{G}_2$ is larger than 0). There are two methods for asserting system stability [22]. The first one is that the feedback system is stable if

$$\nu_F\left[\mathbf{G}_1(s),\omega\right]+\rho_F\left[\mathbf{G}_2(s),\omega\right]>0,\forall\omega\in[0,\infty]. \tag{13}$$

The second method is that the feedback system is stable if

$$\rho_F\left[\mathbf{G}_1(s),\omega\right]+\nu_F\left[\mathbf{G}_2(s),\omega\right]>0,\forall\omega\in[0,\infty]. \tag{14}$$

In this way, the conservativeness of the original passivity-based stability condition is reduced, allowing the passivity-based theory to be applicable even if some subsystems are not passive. For grid-connected inverter system $[\mathbf{Y}, \mathbf{Z}_g]$, the extended passivity-based stability conditions introduced in (13) and (14) are also applicable. Compared to the stability conditions in (7) or (10), those in (13) and (14) are less conservative since they do not require the inverter to be passive.

IV. Limitation 1: Inappropriate Selection of Passivity Index-Based Stability Conditions

A. Two Passivity Index-Based Stability Conditions in Grid-Connected Inverter Systems

When the system in Fig. 2 is modeled as $[\mathbf{Y}, \mathbf{Z}_g]$, the negative-feedback system is stable when it satisfies the requirements in (13)

$$\nu_F\left[\mathbf{Y}(s),\omega\right]+\rho_F\left[\mathbf{Z}_g(s),\omega\right]>0,\forall\omega\in[0,\infty] \tag{15}$$

or in (14)

$$\rho_F\left[\mathbf{Y}(s),\omega\right]+\nu_F\left[\mathbf{Z}_g(s),\omega\right]>0,\forall\omega\in[0,\infty]. \tag{16}$$

Similarly, when the system in Fig. 2 is modeled as $[\mathbf{Z}_g^{-1}, \mathbf{Y}^{-1}]$, the negative-feedback system should be stable when it satisfies (13)

$$\nu_F\left[\mathbf{Y}^{-1}(s),\omega\right]+\rho_F\left[\mathbf{Z}_g^{-1}(s),\omega\right]>0,\forall\omega\in[0,\infty] \tag{17}$$

or (14)

$$\rho_F\left[\mathbf{Y}^{-1}(s),\omega\right]+\nu_F\left[\mathbf{Z}_g^{-1}(s),\omega\right]>0,\forall\omega\in[0,\infty]. \tag{18}$$

According to the definitions of (11) and (12), it is easy to conclude that

$$\nu_F\left[\mathbf{Y}(s),\omega\right]=\rho_F\left[\mathbf{Y}^{-1}(s),\omega\right] \tag{19}$$

$$\nu_F\left[\mathbf{Z}_g(s),\omega\right]=\rho_F\left[\mathbf{Z}_g^{-1}(s),\omega\right]. \tag{20}$$

Upon substituting (19) and (20) to (17) and (18), it can be seen that (15) is equivalent to (18) and (16) is equivalent to (17). Therefore, it is sufficient to consider the case of $[\mathbf{Y}, \mathbf{Z}_g]$ to cover all situations. It is clear that (15) and (16) are two distinct methods, with different requirements for the index of $\mathbf{Y}$. Equation (15) necessitates the calculation of the IFP index of $\mathbf{Y}$, while (16) requires the OFP index of $\mathbf{Y}$. However, the aforementioned conditions in (15) and (16) are based on the premise that both $\mathbf{Y}$ and $\mathbf{Z}_g$ are stable and minimum-phase. When $\mathbf{Y}$ fails to meet this prerequisite, yet we still let the system satisfy (15) or (16), the corresponding implications remain undisclosed.

B. Erroneous Selection of Stability Conditions Ignoring the Nonminimum-Phase Characteristics of Inverter Admittance

To reveal the distinctions and limitations resulting from the choice of different passivity index-based stability conditions, how the satisfaction of (15) or (16) guarantees system stability needs to be explored.

When (15) holds, it can be shown that the Nyquist curve of

$$\det\left[\mathbf{I}+\mathbf{Z}_g(s)\mathbf{Y}(s)\right] \tag{21}$$

does not encircle the origin. Similarly, when (16) holds, it can be shown that the Nyquist plot of

$$\det\left[\mathbf{I}+\mathbf{Z}_g^{-1}(s)\mathbf{Y}^{-1}(s)\right] \tag{22}$$

does not encircle the origin. The detailed proof is placed in the Appendix.

For the grid-connected inverter system, a necessary and sufficient condition for system stability is that the closed-loop system does not contain right-half-plane (RHP) poles. According to

Skogestad and Postlethwaite's [24] work, the zeros of (21) and (22) are the poles of the closed-loop system. Therefore, if the determinants have no RHP zeros, the system is stable. However, the fact that the Nyquist curve of (21) and (22) does not encircle the origin does not directly imply that the closed-loop system is stable. The encirclement of the origin is determined by $P_{\text{cl}} = N+P_{\text{ol}}$, where P_{cl} represents the number of RHP poles of the closed-loop system, N is the number of clockwise encirclements of the origin by the Nyquist plot of det $[\mathbf{I} + \mathbf{L}(j\omega)]$, and P_{ol} denotes the number of open-loop unstable pole in $\mathbf{L}$. Here, it is assumed that there is no cancellation of poles and zeros between the physical grid impedance and the inverter system. When $N = 0$, to ensure that P_{cl} is also 0, P_{ol} must be 0.

For (21), $\mathbf{L}$ is $\mathbf{Z}_g\mathbf{Y}$. For (22), $\mathbf{L}$ is $\mathbf{Z}_g^{-1}\mathbf{Y}^{-1}$. For different $\mathbf{L}$, the number of open-loop unstable poles is also different. When $\mathbf{L} = \mathbf{Z}_g\mathbf{Y}$, P_{ol} is determined by both $\mathbf{Y}$ and $\mathbf{Z}_g$. However, since $\mathbf{Z}_g$ itself is passive physically and does not contain any RHP poles, the RHP poles of $\mathbf{L}$ are equal to the RHP poles of $\mathbf{Y}$. In this case, if $\mathbf{Y}$ is stable, there are no RHP poles in $\mathbf{L}$, then det $[\mathbf{I} + \mathbf{L}(j\omega)]$ not encircling the origin implies no RHP pole in the closed-loop system, which in turn implies system stability. On the other hand, when $\mathbf{L} = \mathbf{Z}_g^{-1}\mathbf{Y}^{-1}$, P_{ol} is determined by $\mathbf{Y}^{-1}$ since $\mathbf{Z}_g$ is passive and hence minimum phase. In this case, $\mathbf{Y}$ does not need to be stable; instead, $\mathbf{Y}$ should be the minimum phase. This is because the RHP poles of $\mathbf{Y}^{-1}$ are equal to the RHP zeros of $\mathbf{Y}$. Hence if $\mathbf{Y}$ is a minimum-phase system, det $[\mathbf{I} + \mathbf{L}(j\omega)]$ not encircling the origin implies no RHP poles in the closed-loop system, and the system is stable.

To ensure the correct application of the stability conditions given in (15) and (16), the grid-connected inverter system must meet the corresponding requirements. Since these requirements are mathematical, limitation 1 is general and is not affected by grid conditions, the inverter control structure and parameters, or operating conditions. Generally, when the inverter is modeled as a current source model in parallel with admittance $\mathbf{Y}$, no matter the inverter is PLL-synchronized or PC-synchronized, it is relatively easy to ensure the stability of $\mathbf{Y}$. However, ensuring a minimum phase $\mathbf{Y}$ is more difficult. As has been reported and observed in [16], [21], and [23], $\mathbf{Y}$ has RHP zeros that are difficult to be eliminated. If $\mathbf{Y}$ is a nonminimum phase system, and if (16) holds with $N = 0$, the number of RHP poles in the closed-loop system is equal to the number of RHP poles of the open-loop and the system must be unstable. To avoid potential risks, it is essential to examine the zeros in $\mathbf{Y}$, and using (16) requires extra caution.

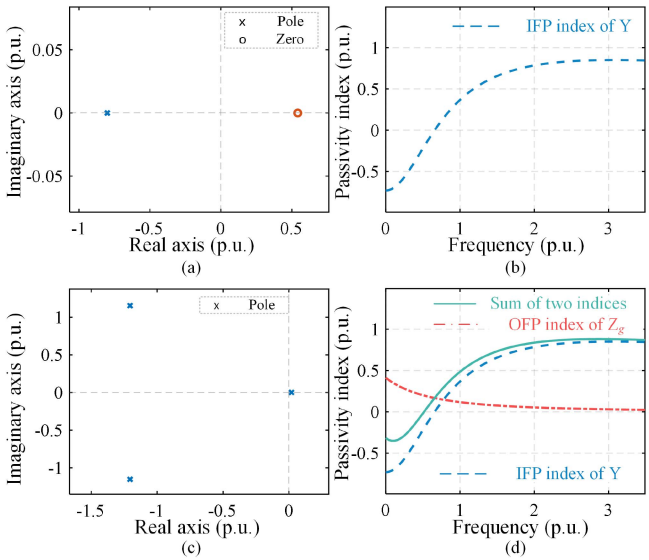

Fig. 7. Numerical example when (15) does not hold. (a) Pole-zero map of $\mathbf{Y}$. (b) IFP index of $\mathbf{Y}$. (c) Pole map of the closed-loop system. (d) Passivity indices of $\mathbf{Y}$ and $\mathbf{Z}_g$.

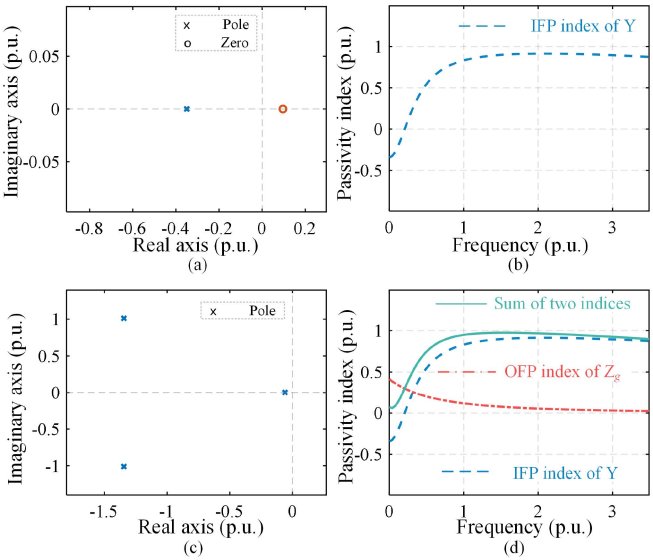

Fig. 8. Numerical example when (15) holds. (a) Pole-zero map of $\mathbf{Y}$. (b) IFP index of $\mathbf{Y}$. (c) Pole map of the closed-loop system. (d) Passivity indices of $\mathbf{Y}$ and $\mathbf{Z}_g$.

C. Numerical Examples

Figs. 7– 10 provide four numerical examples to intuitively illustrate the differences resulting from choosing conditions (15) and (16) when ignoring the nonminimum phase characteristics of $\mathbf{Y}$. In Fig. 7, the filter inductance L, grid inductance L_g, grid resistance R_g, desired CC bandwidth α_c, PLL bandwidth α_p, R_a, G_{ad}, G_{aq}, α_a, and K_v active power P are set to 0.08, 0.9, 0.4, 0, 10.0, 0.8, 2.0, 2.0, 0.2, and 1.0 p.u., respectively. In Fig. 7(a), the zero-pole plot of the system is shown, indicating that $\mathbf{Y}$ is a nonminimum phase system. Fig. 7(b) presents the IFP index of $\mathbf{Y}$, showing the presence of a negative region at low frequencies. Fig. 7(c) shows the zero-pole plot of the closed-loop system, revealing the existence of a pole in the RHP. In this case, the system is unstable. Fig. 7(d) illustrates the relationship between passivity indices in (15), indicating that in the low-frequency range, the sum of the indices for $\mathbf{Y}$ and $\mathbf{Z}_g$ is less than zero, implying a risk of instability in this frequency range, corresponding to the result in Fig. 7(c).

In Fig. 8, while keeping the other parameters the same, the PLL bandwidth is reduced to 0.35 p.u. In this situation, $\mathbf{Y}$ remains a nonminimum phase system. However, from Fig. 8(d),

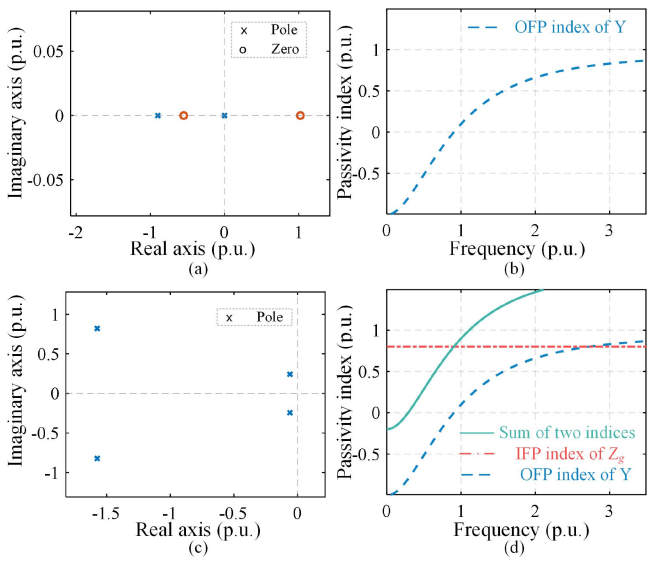

Fig. 9. Numerical example when (16) does not hold. (a) Pole-zero map of **Y**. (b) OFP index of **Y**. (c) Pole map of the closed-loop system. (d) Passivity indices of **Y** and $\mathbf{Z}_g$.

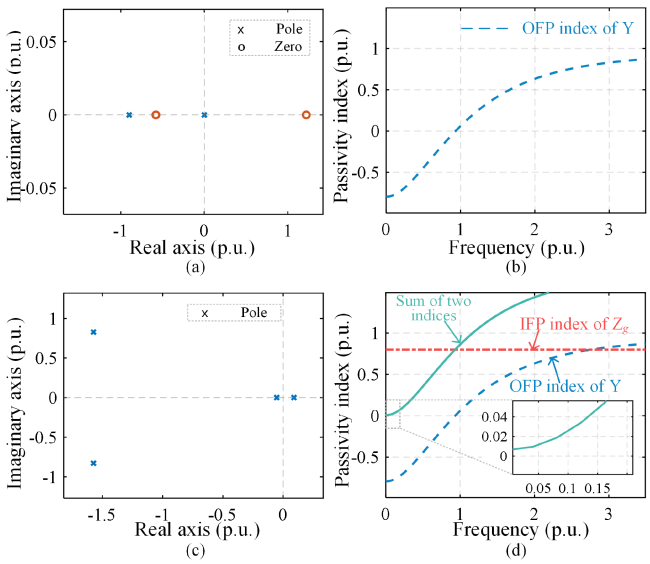

Fig. 10. Numerical example when (16) holds. (a) Pole-zero map of **Y**. (b) OFP index of **Y**. (c) Pole map of the closed-loop system. (d) Passivity indices of **Y** and $\mathbf{Z}_g$.

it can be observed that the excessive passivity in grid impedance can compensate for the lack of passivity in **Y** at low frequencies. The system satisfies (15), and thus, the system is stable. The assessments of system stability in Fig. 8(c) and (d) are consistent in this case. Fig. 9 provides an example related to (16). The PLL bandwidth, AVC gain, R_g, and active power are set to 0.88 p.u., $1/R_a$, 0.8 p.u., and 0.8 p.u., respectively. In this case, according to the results in Fig. 9(d), the relationship between IFP and OFP does not satisfy (16). Fig. 9(c) shows that the system is stable in this scenario, which is reasonable. Meeting (16) is only a sufficient condition for system stability. If it is not met, it does not necessarily mean that the system is unstable. In Fig. 10, the active power of the system is increased to 1.0 p.u., and it can be observed that the minimum value of OFP for **Y** is improved. Under the same grid conditions, the system satisfies (16). However, due to the presence of an RHP zero in **Y**, meeting condition (16) implies the existence of RHP poles in the closed-loop system, indicating system instability.

V. Limitation 2: Conflicts Between Different Passivity Index Tuning Methods

A. *Inability to Satisfy Passivity-Based Stability Conditions in Practice*

For grid-connected inverter systems, it is often challenging to satisfy passivity-based stability conditions, even in their reduced conservativeness versions given in Section IV-A. There are two reasons. One reason for this is that the passivity index of the inverter is inherently nonpositive at low frequencies [1], [16]. Taking the PLL-synchronized inverter as an example, according to Chen et al. [25], the expressions of its input admittance matrix ($[Y_{dd}, Y_{qd}; Y_{dq}, Y_{qq}]$) without considering time delay are as follows:

$$\begin{aligned} Y_{dd} &= \frac{R_a}{sL+R_a} G_{ad} + \frac{1}{sL+R_a}\frac{s}{s+\alpha_f} \\ Y_{qd} &= \frac{R_a}{sL+R_a}\frac{i_{q0}}{E_0}\frac{\alpha_p}{s+\alpha_p} \\ Y_{dq} &= -\frac{R_a}{sL+R_a}\frac{K_v}{s} \\ Y_{qq} &= \frac{R_a}{sL+R_a}\left(G_{aq}\frac{s}{s+\alpha_p} - \frac{i_{d0}}{E_0}\frac{\alpha_p}{s+\alpha_p}\right) + \frac{1}{sL+R_a}\left(\frac{s}{s+\alpha_f}\frac{s}{s+\alpha_p}\right) \end{aligned} \tag{23}$$

where i_{d0}, i_{q0}, and E_0 are the steady-state operating point parameters. L and L_g are the line parameters, including the filter and grid impedance. R_a, α_f, α_p, K_v, G_{ad}, and G_{aq} are the controller parameters, which are specifically discussed in Section II. The positions of the physical parameters and control parameters are illustrated in Figs. 2 and 3, respectively. In the case where the AVC is not adopted (K_v is 0), Y_{dq} is 0, and when s approaches 0, other elements can be approximated by

$$\begin{aligned} Y_{dd}(j\omega) &\approx G_{ad} \\ Y_{qd}(j\omega) &\approx i_{q0}/E_0 \\ Y_{qq}(j\omega) &\approx -i_{d0}/E_0. \end{aligned} \tag{24}$$

The IFP index of **Y** can be calculated as

$$\nu_F \approx \frac{1}{2}\left(G_{ad} - \frac{i_{d0}}{E_0} - \sqrt{\left(G_{ad} + \frac{i_{d0}}{E_0}\right)^2 + \left(\frac{i_{q0}}{E_0}\right)^2}\right) \le 0. \tag{25}$$

It should be noted that the approximation in (24) is obtained by substituting $s = j0$ into (23). Therefore, the expression in (25) accurately represents the passivity index value at $\omega = 0$. The use of the approximate symbol here leverages the property of the passivity index at $\omega = 0$ to approximate its value near $\omega = 0$, thereby making the inherent nondissipative characteristics at low frequencies more analytically intuitive. All passivity index plots in this article are drawn using the exact admittance expressions without any approximations. If active power or reactive power injection is not equal to zero, the IFP index

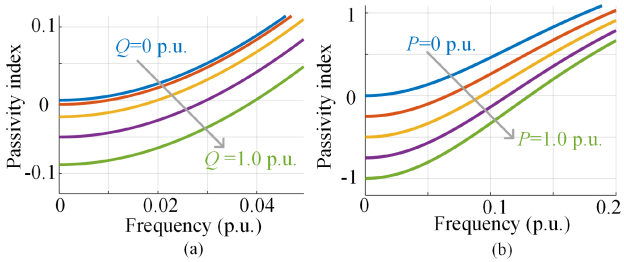

Fig. 11. Passivity index variation of PLL-synchronized inverter. (a) With reactive power. (b) With active power.

TABLE I
PARAMETERS OF CASE 1–CASE 3

Case	G_a(p.u.)	α_a(p.u.)	K_v(p.u.)
1	0.6	0.2	0
2	0.9	0.05	0
3	0.9	0.05	1.5

of $\mathbf{Y}$ becomes negative in the low-frequency range, as shown in Fig. 11. Therefore, to satisfy (15), the grid impedance must provide additional passivity. Since grid impedance is typically composed of *RLC* components, it is straightforward to obtain passivity indices of 0 for both *L* and *C* based on the definitions. Hence, excessive passivity in grid impedance mainly refers to the resistance in the lines. However, in grid-connected inverter systems, the exact value of the grid impedance, including line resistance, is unknown generally. Moreover, adding extra resistance to the line to improve system stability is rarely practical as it would increase active power losses. Considering the previous, the excessive passivity in grid impedance, as shown in Fig. 3, is usually considered to be 0. The above-mentioned conundrum makes it not a feasible goal to satisfy (15) in practice.

B. Inconsistent Results Arising From Two Different Passivity Index Tuning Methods

The objective has to be modified to make $\mathbf{Y}$ closer to passive, and the degree of closeness is characterized by the passivity index. To compare which set of control designs will make $\mathbf{Y}$ closer to being passive, there are two perspectives. An intuitive idea is to enhance system stability robustness by reducing the nondissipative frequency region of $\mathbf{Y}$ [6]. Another approach is to alleviate the passivity deficiency, meaning to increase the minimum value of the passivity index [16]. Many examples demonstrating the effectiveness of these two methods have been provided in previous studies, and the following examples will focus specifically on potential issues.

Fig. 12 presents three cases involving PC-synchronized inverters, where the Q-V droop gain, α_c, α_f, L, and active power are set to 0.03, 8.0, 8.0, 0.08, and 1.0 p.u., respectively. The primary parameter distinctions among these three examples are presented in Table I. In Fig. 12, it is evident that Case 2 exhibits a noticeably "better" passivity index compared to Case 1. From the negative region perspective, Case 2 has a narrower negative region. In terms of the minimum value of the passivity index, Case 2 has a higher value. Therefore, from either perspective, it

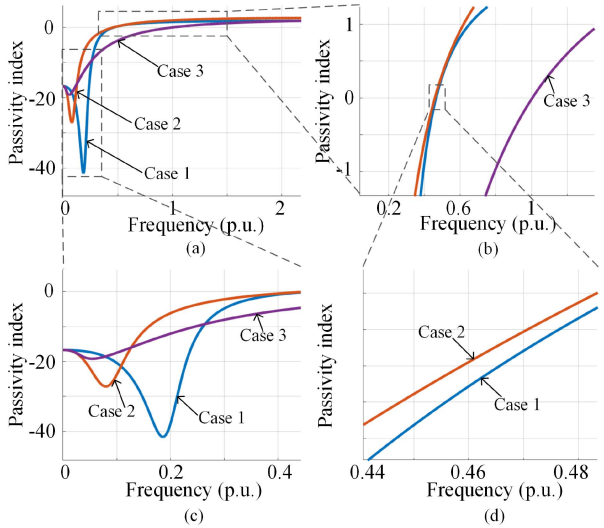

Fig. 12. Control design that is based on improving the passivity index. (a) Comparison among the passivity indices of Case 1 to Case 3. (b) Zooming. (c) Zooming. (d) Zooming.

can be considered that Case 2 is a better design (as it is expected to give rise to better stability robustness). Comparing Case 2 and Case 3, it can be observed that Case 2 has a better design from the perspective of the negative region. However, on the other hand, the minimum value of the passivity index in Case 3 is larger than that in Case 2. A conflict arises between the two methods mentioned previously in Fig. 12. In situations such as Case 2 and Case 3, to the best of our knowledge, there is no reliable method to determine which design enables better closed-loop system stability robustness.

VI. LIMITATION 3: INSUFFICIENT RELATIONSHIP BETWEEN A NARROWER NEGATIVE PASSIVITY INDEX FREQUENCY RANGE AND ENHANCED STABILITY ROBUSTNESS

A. Integrator-Induced Passivity Index Divergence

In some cases, it is not practical to improve the passivity from the perspective of increasing the minimum values of the indices. For example, when the AVC gain in Fig. 3(a) is not zero and the Q-V droop in Fig. 3(b) is absent, as s approaches 0, the IFP index of $\mathbf{Y}$ will tend toward negative infinity. In (23), if an integral AVC is adopted, the input admittance matrix can be approximated as follows within the low-frequency range:

$$\mathbf{Y}(j\omega) = \begin{bmatrix} G_{ad} & i_{q0}/E_0 \\ -jK_v/\omega & -i_{d0}/E_0 \end{bmatrix}, \quad \omega \approx 0 \tag{26}$$

when the frequency is low, K_v/ω is the dominant term. According to (11), the IFP index can be approximated by

$$\nu_F = -\frac{1}{2}\frac{K_v}{\omega} \tag{27}$$

which approaches negative infinity as $\omega \to 0$. When this situation is present, the only passivity degree metric that can be improved is the frequency region of the negative index, as shown in Fig. 13.

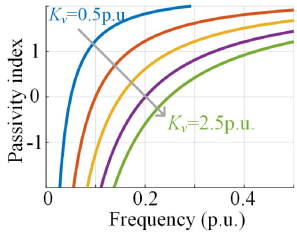

Fig. 13. Impact of K_v on the passivity index.

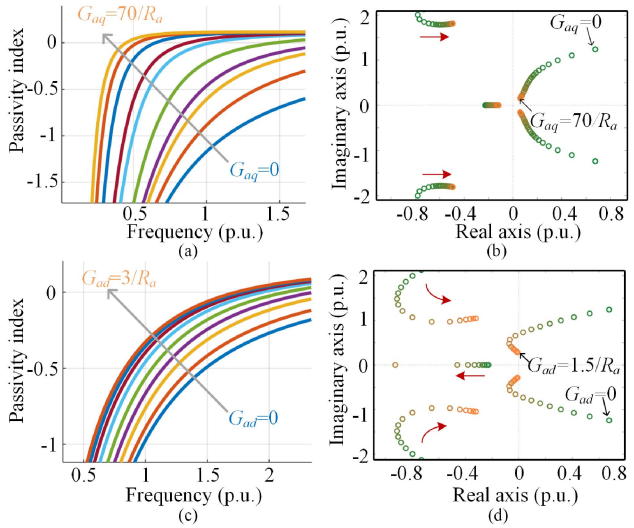

Fig. 14. Misleading control design based on passivity index. (a) Passivity index variation with G_{aq}. (b) Corresponding root locus of the closed-loop system in (a). (c) Passivity index variation with G_{ad}. (d) Corresponding root locus of the closed-loop system in (c).

B. Impact of Narrowing the Negative Passivity Index Frequency Range on Stability Robustness

Fig. 14 shows misleading examples on narrowing the frequency range of negative passivity index on designing d-axis and q-axis active damper for PLL-synchronized inverters, where PLL bandwidth and AVC gain are set as 0.7 and 1.0 p.u. Fig. 14(a) indicates that increasing the AD gain G_{aq} can reduce the frequency region of negative passivity index. However, the root trajectory in Fig. 14(b) shows that the system is still unstable even though the gain has been increased to an unreasonably large value (70 times the recommended value in Harnefors et al.'s [20] work). Fig. 14(c) indicates that increasing the AD gain G_{ad} has a consistently positive impact on the passivity index. However, the root trajectory in Fig. 14(d) shows a nonmonotonic effect, where increasing G_{ad} initially stabilizes the system, but continuing to increase G_{ad} will render the system unstable again in Fig. 14(d).

Two more PLL-synchronized designs are performed with a short circuit ratio of 1.1 and a desired CC loop bandwidth of 12 p.u. in Figs. 15 and 16. The d-axis AD gain, PLL bandwidth are set as 1.0 and 0.5 p.u., respectively. The difference only exists in the AVC. In Fig. 15, the AVC gain K_v is set as 1.5 p.u. while the K_v in Fig. 16 is set as 0.16 p.u. Although Fig. 16 exhibits a "better" passivity index in the sense that the negative

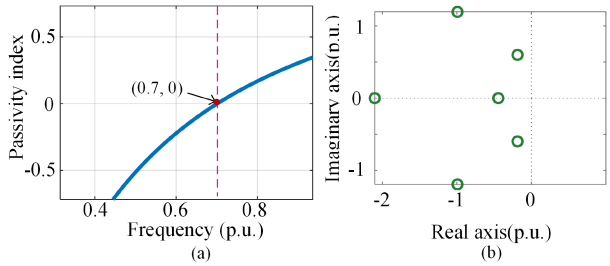

Fig. 15. Stable PLL-based system with wider passivity index. (a) Passivity index. (b) Pole map of the system.

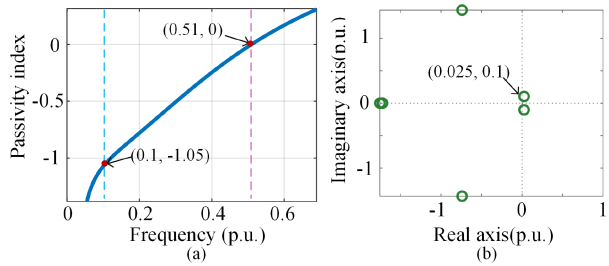

Fig. 16. Unstable PLL-based system with narrower passivity index. (a) Passivity index. (b) Pole map of the system.

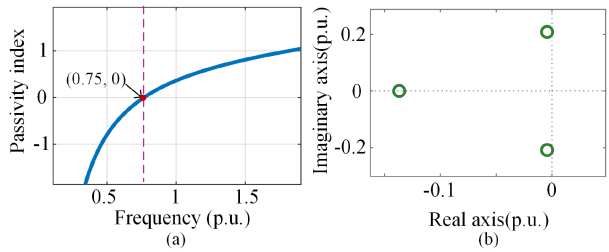

Fig. 17. Stable PC-based system with wider passivity index for. (a) Passivity index. (b) Pole map of the system.

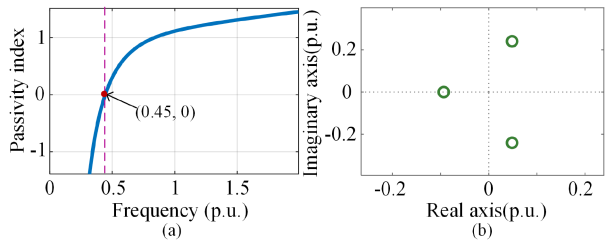

Fig. 18. Unstable PC-based system with wider passivity index for. (a) Passivity index. (b) Pole map of the system.

region is narrower, the poles of the system reveal an opposite conclusion. In fact, despite having a "better" passivity index, Fig. 16 is unstable, whereas Fig. 15 is stable.

Figs. 17 and 18 show two PC-synchronized inverter designs, where the filter inductance L, grid inductance L_g, grid resistance R_g, desired CC bandwidth α_c, PC gain K_p, R_a, G_{ad}, G_{aq}, α_a, active power P are set to 0.08, 0.1, 0.0, 6.0, 2.0, 0.48, 1.8, 1.8, 0.2, and 1.0 p.u., respectively. K_v in Fig. 17 is set as 0.0 p.u. while

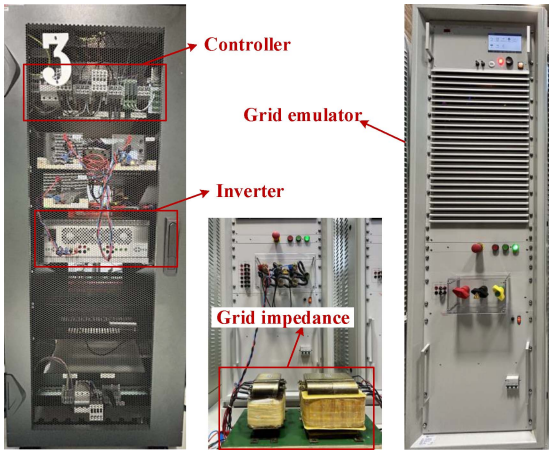

Fig. 19. Experimental platform.

K_v in Fig. 18 is set as 2.0 p.u. Like the cases in Figs. 15 and 16, In Fig. 17, the index has a wider negative region but the system remains stable, while in Fig. 18, with a narrower negative region, it is unstable. The above-mentioned discussion indicates that destabilization of the system typically does not occur in regions with positive indices. Therefore, the negative index region can serve as an indicator of potential intervals where instability may occur. However, it is important to clarify that in the examples given previously, narrowing the negative index region merely suggests that the frequency intervals at which instability may occur have become narrower. This does not necessarily imply a reduction in the probability of instability occurring.

Unlike the cause of limitation 1, the root cause of limitations 2 and 3 is that the passivity-based stability condition is only a sufficient condition for system stability. Once the suitable passivity index is selected, as discussed in limitation 1, if any of the conditions in (15)–(18) are met, the system is undoubtedly stable. However, when a sufficient condition is not met, logically, the system can be either stable or unstable. This means that the two passivity index tuning methods discussed in limitation 2 do not correlate with system stability. Compared to the traditional eigenvalue-based analysis method, passivity theory does not offer a significant advantage. Therefore, to avoid incorrect analysis results, it is not recommended to use passivity theory in the low-frequency range.

VII. Experimental Results

To verify the correctness of the theoretical and numerical analysis, experimental tests are conducted. The experimental platform is shown in Fig. 19, which mainly includes the inverter, output filter, grid impedance, and the grid itself. The inverter side uses back-to-back converters, allowing the dc-bus voltage to be controlled independently from the other converter. The inverter output is filtered using an inductive–capacitive (*LC*) filter. The grid impedance is purely inductive, and the grid is formed by a grid simulator. The system and controller parameters are listed in Table II. Normalization to per-unit (p.u.) variables and parameters is done here. This is because p.u. values are generic and apply to both small and large converters (in terms of voltage and power).

TABLE II
Parameters of the Experimental Platform and the Controllers

Parameters	Strong grid (p.u.)	Weak grid (p.u.)
Rated power	2 kVA (1.0)	2 kVA (1.0)
Rated voltage	110 V (1.0)	110 V (1.0)
Rated current	8.57 A (1.0)	8.57 A (1.0)
Based impedance	18.15 Ω (1.0)	18.15 Ω (1.0)
Filter inductance L	4 mH (0.07)	4 mH (0.07)
Filter capacitance C	10 μF (0.06)	10 μF (0.06)
Grid impedance L_g	6 mH (0.103)	48 mH (0.824)
Fundamental frequency	50 Hz (1.0)	50 Hz (1.0)
Switching frequency	10k Hz (200)	10k Hz (200)
Bandwidth of CC	800π rad/s (8.0)	1400π rad/s (14.0)
α_f	200π rad/s (2.0)	800π rad/s (8.0)

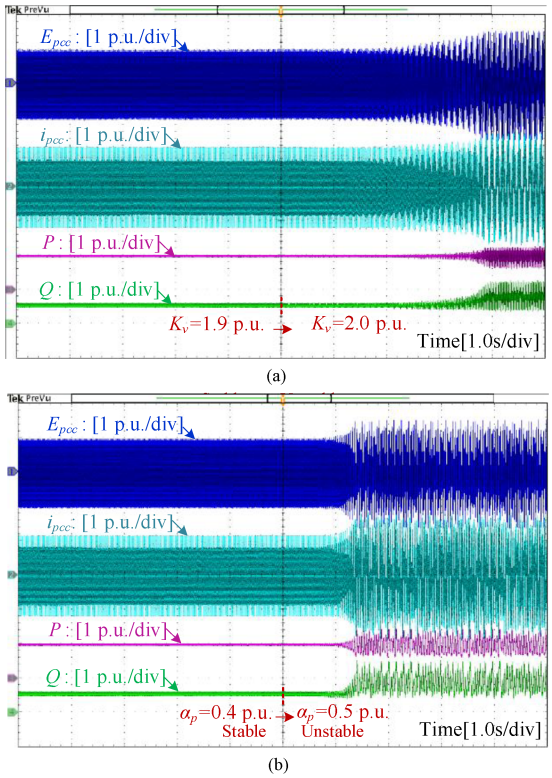

Fig. 20. Experimental results of PLL-synchronized inverter. (a) Increasing AVC gain. (b) Increasing PLL bandwidth.

Two different grid conditions (strong grid and weak grid) and two types of inverter control (PLL-synchronized and PC-synchronized), are tested. A grid inductance of 1 p.u. means that the converter can barely inject its rated power into the grid as seen from its connecting point, indicating a very weak grid. Here, the value of L_g in a weak grid is considered as 0.824 p.u., providing a small margin to the rated power. Grids are considered to be very strong if $L_g < 0.2$ p.u. [20]. Here, L_g is set to 0.103 p.u. to simulate a strong grid condition. The design of the inverter parameters is based on the conclusions discussed in [20] and [26]. Moreover, all experiments are repeated three times on different dates to avoid the influence of random factors.

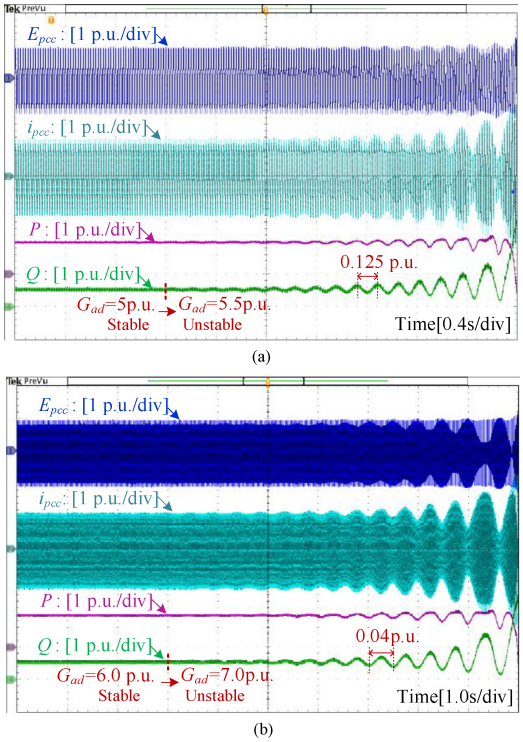

Fig. 21. Experimental results of PLL-synchronized inverter when increasing G_{ad}. (a) G_{aq}=1.0 p.u. (b) G_{aq}=10.0 p.u.

Fig. 20 shows the experimental waveforms of a PLL-synchronized inverter in a weak grid condition. In Fig. 20(a), the system becomes unstable when increasing the AVC gain K_v. As discussed in (26) and (27), in this case, the only passivity index tuning method is to narrow the frequency range where the inverter is nondissipative. According to Fig. 13, increasing K_v enlarges the frequency region of the negative index. Therefore, the waveforms in Fig. 20(a) indicate that, for the case of varying AVC gain K_v, narrowing the nondissipative region of the inverter to improve the stability robustness is effective. Fig. 20(b) shows the system instability caused by increasing the PLL bandwidth. According to Harnefors et al.'s [6] work, increasing the PLL bandwidth enlarges the nondissipative region. Thus, for the PLL bandwidth, narrowing the nondissipative region of the inverter is also effective in improving system stability robustness.

Fig. 21 shows the experimental waveforms of a PLL-synchronized inverter in a weak grid condition. The PLL bandwidth is set as 0.2 p.u., with (a) and (b) representing waveforms when increasing AD gains. In Fig. 14, it is shown that either increasing the G_{ad} or G_{aq} can reduce the frequency region of the negative index. In Fig. 21(a), G_{aq} is set as 1.0 p.u., and as G_{ad} gradually increased from 5 to 5.5 p.u., the system exhibits low-frequency oscillations with a frequency of 0.125 p.u. This demonstrates that narrowing the frequency region of the negative index does not necessarily imply greater stability robustness. In (b), G_{aq} is set to 10 p.u., and as G_{ad} increased from 6 to 7 p.u., the system experiences extremely low-frequency oscillations, specifically at 0.04 p.u.

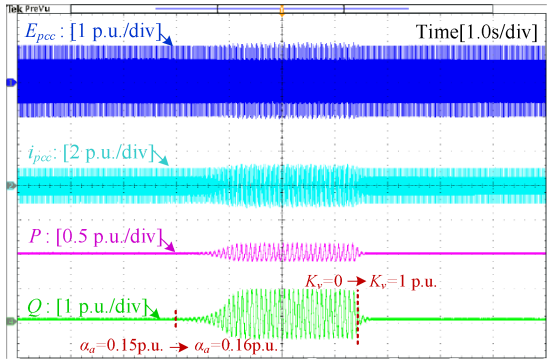

Fig. 22. Experimental results of PC-synchronized inverter when increasing K_v.

Fig. 22 shows the measured waveforms of a PC-synchronized inverter in strong grid conditions. Initially, oscillations are induced in the system by increasing α_a, and then K_v is gradually increased from 0 to 1 p.u. From Figs. 17 and 18, it can be observed that increasing K_v expands the frequency region of the negative index. However, after increasing K_v, it can be seen from Fig. 22 that the system transitions from instability to stability. The comparison between Figs. 20 and 21 and the results in Fig. 22 show that the passivity index tuning method is not consistently effective. Even within the same control architecture, different parameters can affect the effectiveness of the passivity index tuning method. This validates the discussion in Section VI, which states that the passivity-based stability condition is a sufficient condition for system stability. When this sufficient condition is not met, the system can be either stable or unstable.

VIII. Conclusion

Passivity theory has been demonstrated as effective through extensive studies in analyzing grid–inverter interactions. However, due to the unignorable asymmetric dynamics of grid-connected inverters in the low-frequency region, there are limitations to the passivity theory-based analysis. First, the nonminimum phase characteristics of the inverter admittance need to be taken into account; otherwise, erroneous stability conclusions may be reached. Subsequently, two passivity index tuning methods, including reducing the nondissipative frequency region and increasing the minimum value of the passivity index, have been found to potentially yield inconsistent results. Finally, the common perception associating a narrower negative passivity index frequency range with enhanced system robustness has been found to lead to misguided designs, resulting in low-frequency oscillations in the system.

Given matrix $\mathbf{M} \in \mathbb{C}^{n\times n}$, its complex conjugate transpose is denoted by $\mathbf{M}^H$. $\mathbf{M}$ is said to be Hermitian if $\mathbf{M} = \mathbf{M}^H$. When this is the case, $\mathbf{M} > xI$ for some $x \in \mathbb{R}$ denotes $\min\lambda[\mathbf{M}] > x$, where λ denotes the spectrum of $\mathbf{M}$. $\mathbf{M}$ is said to be positive definite if $\mathbf{M} > 0$.

To prove that based on (15), (21) does not encircle the origin, a close examination of the IFP index of $\mathbf{Y}$ and the OFP index of $\mathbf{Z}_g$ is required. Taking grid resistance R_g into consideration, $\mathbf{Z}_g$

is expressed as

$$\mathbf{Z}_g = \begin{bmatrix} R_g + sL_g & -\omega_1 L_g \\ \omega_1 L_g & R_g + sL_g \end{bmatrix}. \tag{28}$$

At a certain frequency ω, the eigenvalues of $\mathbf{Z}_g(j\omega)$ can be obtained

$$\lambda_{1,2} = R_g + j\omega L_g \pm j\omega_1 L_g.$$

$\mathbf{Z}_g(j\omega)$ is non-singular since $\lambda_{1,2} \neq 0$. Hence $\det(\mathbf{Z}_g) \neq 0$. Denote the value of the OFP index of $\mathbf{Z}_g$ at frequency ω as $0.5\,k > 0$ as in Bao et al.'s [[22], (2.88) and (2.99)] work, from which it follows that:

$$\mathbf{Z}_g^{-1}(j\omega) + \mathbf{Z}_g^{-H}(j\omega) = kI. \tag{29}$$

Since (15) holds, based on (29) and (15), it can be obtained that the value of the IFP index of $\mathbf{Y}$ is larger than $-0.5k$. Hence

$$\mathbf{Y}(j\omega) + \mathbf{Y}^H(j\omega) > -kI. \tag{30}$$

Moreover, according to (29), it is easy to obtain that

$$\kappa\mathbf{Z}_g^{-1}(j\omega) + \kappa\mathbf{Z}_g^{-H}(j\omega) \geq kI \tag{31}$$

holds for any $\kappa \geq 1$. Then

$$\mathbf{Y}(j\omega) + \mathbf{Y}^H(j\omega) + \kappa\mathbf{Z}_g^{-1}(j\omega) + \kappa\mathbf{Z}_g^{-H}(j\omega) > 0. \tag{32}$$

According to the Lemma 1 in Griggs et al.'s [27] work, when (32) holds, it can be obtained that

$$\det\left[\kappa\mathbf{Z}_g^{-1}(j\omega) + \mathbf{Y}(j\omega)\right] \neq 0. \tag{33}$$

Then

$$\det\left[I + \frac{1}{\kappa}\mathbf{Z}_g(j\omega)\,\mathbf{Y}(j\omega)\right] \neq 0 \tag{34}$$

since $\det[\kappa\mathbf{Z}_g^{-1}(j\omega) + \mathbf{Y}(j\omega)]$ equals to

$$\det\left[\tfrac{1}{\kappa}\mathbf{Z}_g(j\omega)\right]\det\left[\kappa\mathbf{Z}_g^{-1}(j\omega) + \mathbf{Y}(j\omega)\right] \tag{35}$$

and $\mathbf{Z}_g$ is nonsingular. According to Theorem 8.1 in Skogestad and Postlethwaite's [24] work, if (34) holds for all $\omega \geq 0$ and $\kappa \geq 1$, then the Nyquist plot of (21) does not encircle the origin. The proof to show based on (16), the Nyquist plot of (22) does not encircle the origin is a symmetric process from (29) to (35), which will not be repeated here.

REFERENCES

[1] M. Beza and M. Bongiorno, "Identification of resonance interactions in offshore-wind farms connected to the main grid by MMC based HVDC system," *Int. J. Elect. Power Energy Syst.*, vol. 111, pp. 101–113, Oct. 2019.

[2] C. Li, J. Liang, L. M. Cipcigan, W. Ming, F. Colas, and X. Guillaud, "DQ impedance stability analysis for the power-controlled grid-connected inverter," *IEEE Trans. Energy Convers.*, vol. 35, no. 4, pp. 1762–1771, Dec. 2020.

[3] L. Huang et al., "Gain and phase: Decentralized stability conditions for power electronics-dominated power systems," *IEEE Trans. Power Syst.*, early access, Mar. 21, 2024, doi: 10.1109/TPWRS.2024.3380528.

[4] C. Hirsching et al., "Passivity-based sensitivity analysis of the inner current controller in grid-following MMC-HVDC applications - an overview," in *Proc. 46th Annu. Conf. IEEE Ind. Electron. Soc.*, 2020, pp. 1412–1417.

[5] L. Harnefors, M. Bongiorno, and S. Lundberg, "Input-admittance calculation and shaping for controlled voltage-source converters," *IEEE Trans. Ind. Electron.*, vol. 54, no. 6, pp. 3323–3334, Dec. 2007.

[6] L. Harnefors, X. Wang, A. G. Yepes, and F. Blaabjerg, "Passivity-based stability assessment of grid-connected VSCs–an overview," *IEEE Trans. Emerg. Sel. Topics Power Electron.*, vol. 4, no. 1, pp. 116–125, Mar. 2016.

[7] L. Harnefors, A. G. Yepes, A. Vidal, and J. Doval-Gandoy, "Passivity-based controller design of grid-connected VSCs for prevention of electrical resonance instability," *IEEE Trans. Ind. Electron.*, vol. 62, no. 2, pp. 702–710, Feb. 2015.

[8] G. Ma, C. Xie, C. Li, J. Zou, and J. M. Guerrero, "Passivity-based design of passive damping for LCL-type grid-connected inverters to achieve full-frequency passive output admittance," *IEEE Trans.Power Electron.*, vol. 38, no. 12, pp. 16048–16060, Dec. 2023.

[9] G. Wu et al., "Passivity-based stability analysis and generic controller design for grid-forming inverter," *IEEE Trans.Power Electron.*, vol. 38, no. 5, pp. 5832–5843, May. 2023.

[10] M. Miranbeigi, P. M. Gajare, J. Benzaquen, P. Kandula, and D. Divan, "On the passivity of grid-forming converters – role of virtual impedance," in *Proc. IEEE Appl. Power Electron. Conf. Expo.*, 2022, pp. 650–656.

[11] M. Beza and M. Bongiorno, "Impact of converter control strategy on low-and high-frequency resonance interactions in power-electronic dominated systems," *Int. J. Elect. Power Energy Syst.*, vol. 120, Sep. 2020, Art. no. 105978.

[12] I. Z. Petric, P. Mattavelli, and S. Buso, "Multi-sampled grid-connected VSCs: A path toward inherent admittance passivity," *IEEE Trans.Power Electron.*, vol. 37, no. 7, pp. 7675–7687, Jul. 2022.

[13] J. Serrano-Delgado, S. Cobreces, M. Rizo, and E. J. Bueno, "Low-order passivity-based robust current control design for grid-tied VSCs," *IEEE Trans.Power Electron.*, vol. 36, no. 10, pp. 11886–11899, Oct. 2021.

[14] Y. Qi, H. Deng, J. Wang, and Y. Tang, "Passivity-based synchronization stability analysis for power-electronic-interfaced distributed generations," *IEEE Trans. Sustain. Energy*, vol. 12, no. 2, pp. 1141–1150, Apr. 2021.

[15] L. Harnefors, X. Wang, S.-F. Chou, M. Bongiorno, M. Hinkkanen, and M. Routimo, "Asymmetric complex-vector models with application to VSC–grid interaction," *IEEE Trans. Emerg. Sel. Topics Power Electron.*, vol. 8, no. 2, pp. 1911–1921, Jun. 2020.

[16] F. Zhao, X. Wang, and T. Zhu, "Low-frequency passivity-based analysis and damping of power-synchronization controlled grid-forming inverter," *IEEE Trans. Emerg. Sel. Topics Power Electron.*, vol. 11, no. 2, pp. 1542–1554, Apr. 2023.

[17] F. Chen, L. Zhao, L. Harnefors, J. Kukkola, M. Routimo, and X. Wang, "Pitfalls of using passivity index to guide grid-connected inverter control design in low-frequency region," in *Proc. IEEE Energy Convers. Congr. Expo.*, 2023, pp. 758–764.

[18] X. Wang, M. G. Taul, H. Wu, Y. Liao, F. Blaabjerg, and L. Harnefors, "Grid-synchronization stability of converter-based resources–an overview," *IEEE Open J. Ind. Appl.*, vol. 1, pp. 115–134, 2020.

[19] B. Wen, D. Boroyevich, R. Burgos, P. Mattavelli, and Z. Shen, "Analysis of D-Q small-signal impedance of grid-tied inverters," *IEEE Trans.Power Electron.*, vol. 31, no. 1, pp. 675–687, Jan. 2016.

[20] L. Harnefors, J. Kukkola, M. Routimo, M. Hinkkanen, and X. Wang, "A universal controller for grid-connected voltage-source converters," *IEEE Trans. Emerg. Sel. Topics Power Electron.*, vol. 9, no. 5, pp. 5761–5770, Oct. 2021.

[21] Y. Liao and X. Wang, "Impedance-based stability analysis for interconnected converter systems with open-loop RHP poles," *IEEE Trans.Power Electron.*, vol. 35, no. 4, pp. 4388–4397, Apr. 2020.

[22] J. Bao, P. L. Lee, and B. E. Ydstie, *Process Control: The Passive Systems Approach*, vol. 805. Berlin, Germany: Springer, 2007.

[23] B. Wen, D. Boroyevich, R. Burgos, P. Mattavelli, and Z. Shen, "Inverse nyquist stability criterion for grid-tied inverters," *IEEE Trans. Power Electron.*, vol. 32, no. 2, pp. 1548–1556, Feb. 2017.

[24] S. Skogestad and I. Postlethwaite, *Multivariable Feedback Control: Analysis and Design*. Hoboken, NJ, USA: John Wiley and Sons, Inc., 2005.

[25] F. Chen, L. Zhao, L. Harnefors, and X. Wang, "Impedance modeling for quadrature-axis active damping of PLL dynamics," in *Proc. IEEE 23rd Workshop Control Modelling Power Electron.*, 2022, pp. 1–7.

[26] F. Chen, L. Zhao, L. Harnefors, X. Wang, J. Kukkola, and M. Routimo, "Enhanced q-axis voltage-integral damping control for fast pll-synchronized inverters in weak grids," *IEEE Trans. Power Electron.*, vol. 39, no. 1, pp. 424–435, Jan. 2024.

[27] W. M. Griggs, S. S. K. Sajja, B. D. O. Anderson, and R. N. Shorten, "On interconnections of "mixed" systems using classical stability theory," *Syst. Control Lett.*, vol. 61, no. 5, pp. 676–682, 2012.

Feifan Chen (Graduate Student Member, IEEE) received the B.S. and M.S. degrees in electrical engineering from the Harbin Institute of Technology, Harbin, China, in 2019 and 2021, respectively. He is currently working toward the Ph.D. degree in electrical engineering with the School of Electrical Engineering and Computer Science, KTH Royal Institute of Technology, Stockholm, Sweden.

His research interests include modeling and control of grid-connected converters, stability assessment and dynamic analysis of power-electronic-dominated power systems.

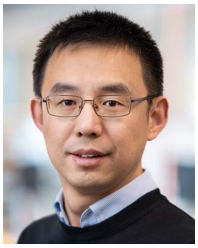

Xiongfei Wang (Fellow, IEEE) received the B.S. degree from Yanshan University, Qinhuangdao, China, in 2006, the M.S. degree from the Harbin Institute of Technology, Harbin, China, in 2008, both in electrical engineering, and the Ph.D. degree in energy technology from Aalborg University, Aalborg, Denmark, in 2013.

From 2009 to 2022, he was with Aalborg University where he became an Assistant Professor in 2014, an Associate Professor in 2016, a Professor and the Founding Leader of Electronic Power Grid (eGRID) Research Group in 2018. From 2022, he has been a Professor with KTH Royal Institute of Technology, Stockholm, Sweden, and a Part-time Professor with Aalborg University. Form 2023, he has been a Visiting Professor with Hitachi Energy Research Center, Vasteras, Sweden. His research interests include modeling and control of power electronic converters, stability and power quality of power-electronic-dominated power systems, and high-power electronic systems.

Dr. Wang was the recipient of ten IEEE Prize Paper Awards, the 2016 AAU Talent for Future Research Leaders, the 2018 IEEE Richard M. Bass Outstanding Young Power Electronics Engineer Award, the 2019 IEEE PELS Sustainable Energy Systems Technical Achievement Award, and the 2022 Isao Takahashi Power Electronics Award. He is an Executive Editor (Editor-in-Chief) for IEEE TRANSACTIONS ON POWER ELECTRONICS LETTERS and an Associate Editor for IEEE JOURNAL OF EMERGING AND SELECTED TOPICS IN POWER ELECTRONICS.

Lennart Harnefors (Fellow, IEEE) received the M.Sc., Licentiate, and Ph.D. degrees in electrical engineering from the Royal Institute of Technology (KTH), Stockholm, Sweden, and the Docent (D.Sc.) degree in industrial automation from Lund University, Lund, Sweden, in 1993, 1995, 1997, and 2000, respectively.

He is a Part-time Visiting Professor with Aalto University, Espoo, Finland. From 1994 to 2005, he was with Malardalen University, Vasteras, Sweden. From 2001, he was a Professor of electrical engineering. From 2001 to 2005, he was a Part-time Visiting Professor of electrical drives with the Chalmers University of Technology, Göteborg, Sweden. In 2005, he joined ABB, HVDC Product Group, Ludvika, Sweden, where, among other duties, he led the control development of the first generation of multilevel-converter HVDC Light. In 2012, he joined ABB, Corporate Research, Västerås, where he was appointed a Senior Principal Scientist in 2013 and a Corporate Research Fellow in 2021. His research interests include control and dynamic analysis of power electronic systems, particularly grid-connected converters and ac drives.

Dr. Harnefors was the recipient of the 2020 IEEE Modeling and Control Technical Achievement Award. He is an Editor for IEEE JOURNAL OF EMERGING AND SELECTED TOPICS IN POWER ELECTRONICS.

Sei Zhen Khong (Senior Member, IEEE) received the bachelor's degree (with first class honours) and the Ph.D. degree from the University of Melbourne, Parkville, VIC, Australia, in 2008 and 2012, respectively, both in electrical engineering.

He is currently with the Department of Electrical Engineering, National Sun Yat-sen University, Kaohsiung, Taiwan. He held research positions with the Department of Electrical and Electronic Engineering, University of Melbourne, Department of Automatic Control, Lund University, Lund, Sweden, the Institute for Mathematics and its Applications, University of Minnesota Twin Cities, Minneapolis-Saint Paul, MN, USA, and the Department of Electrical and Electronic Engineering, University of Hong Kong, Hong Kong. His research interests include network control, systems theory, and optimization with applications to systems biology, power systems, and electromechanical systems.

Dan Wang (Member, IEEE) received the B.S. degree in automation from Hangzhou Dianzi University, Hangzhou, Zhejiang, China, in 2014, and the M.Phil. and Ph.D. degrees in electronic and computer engineering from the Hong Kong University of Science and Technology, Hong Kong, in 2016 and 2020, respectively.

She is currently a Postdoc with the KTH Royal Institute of Technology, Stockholm, Sweden. From January 2018 to July 2018, she was a Visiting Scholar with Coordinated Science Laboratory, University of Illinois at Urbana Champaign, Urbana, IL, USA. Her research interests include systems and control theory, dynamical networks, network science, and control of epidemics.

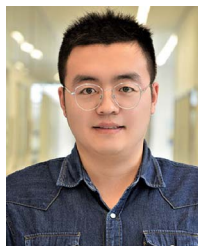

Liang Zhao (Member, IEEE) received the B.S. and M.S. degrees in electrical engineering from the Harbin Institute of Technology, Harbin, China, in 2018 and 2020, respectively, and the Ph.D. degree in power electronic systems from the Department of Energy, Aalborg University, Aalborg, Denmark, in 2024.

He is currently a Postdoctoral Researcher with the KTH Royal Institute of Technology, Stockholm, Sweden. His research interests include modeling and control of power electronic converters and systems.

Dr. Zhao was the recipient of the best paper award for 2023 Wind and Solar Integration Workshop.

Kin Cheong Sou (Member, IEEE) received the Ph.D. degree in electrical engineering and computer science from the Massachusetts Institute of Technology, Cambridge, MA, USA, in 2008.

He is currently an Associate Professor with the Department of Electrical Engineering, National Sun Yat-sen University, Kaohsiung, Taiwan. From 2008 to 2010, he was a Postdoctoral Researcher with Lund University, Lund, Sweden. From 2010 to 2012, he was a Postdoctoral Researcher with the KTH Royal Institute of Technology, Stockholm, Sweden. Between 2013 and 2016, he was an Assistant Professor with the Department of Mathematical Sciences, Chalmers University of Technology, Gothenburg, Sweden, and the University of Gothenburg, Gothenburg, Sweden. His research interests include decision-making and computation techniques for power systems applications.

Mikko Routimo (Member, IEEE) received the M.Sc. (El. Eng.), Lic.Tech., and D.Sc. (Tech.) degrees in electrical engineering from the Tampere University of Technology, Tampere, Finland, in 2002, 2005, and 2009, respectively.

In 2008, he joined ABB Oy Drives, Helsinki, Finland, where he was appointed as a Senior Principal Engineer, in 2022. From 2017 to 2022, he was a Part-time Professor of practice with the School of Electrical Engineering, Aalto University, Espoo, Finland. His research interests include control of grid-connected converters, and power electronics in power systems.

Jarno Kukkola received the B.Sc. (Tech.), M.Sc. (Tech.), and D.Sc. (Tech.) degrees in electrical engineering from the Aalto University, Espoo, Finland, in 2010, 2012, and 2017, respectively.

He is currently an R&D Principal Engineer with ABB Oy Drives, Helsinki, Finland. His research interests include control systems and grid-connected converters.

Henrik Sandberg (Fellow, IEEE) received the M.Sc. degree in engineering physics and the Ph.D. degree in automatic control from Lund University, Lund, Sweden, in 1999 and 2004, respectively.

He is currently a Professor with the Division of Decision and Control Systems, KTH Royal Institute of Technology, Stockholm, Sweden. From 2005 to 2007, he was a Postdoctoral Scholar with the California Institute of Technology, Pasadena, CA, USA. In 2013, he was a Visiting Scholar with the Laboratory for Information and Decision Systems, MIT, Cambridge, MA, USA. He has also held visiting appointments with Australian National University, Canberra, ACT, Australia, and the University of Melbourne, Parkville, VIC, Australia. His research interests include security of cyber–physical systems, power systems, model reduction, and fundamental limitations in control.

Dr. Sandberg was a recipient of the Best Student Paper Award from the IEEE Conference on Decision and Control in 2004, an Ingvar Carlsson Award from the Swedish Foundation for Strategic Research in 2007, and a Consolidator Grant from the Swedish Research Council in 2016. He has served on the editorial boards of IEEE TRANSACTIONS ON AUTOMATIC CONTROL and the *IFAC Journal Automatica*.

Karl Henrik Johansson (Fellow, IEEE) received the M.Sc. degree in electrical engineering and the Ph.D. degree in automatic control from Lund University, Lund, Sweden, in 1992 and 1997, respectively.

He is the Swedish Research Council Distinguished Professor in electrical engineering and computer science with the KTH Royal Institute of Technology, Stockholm, Sweden, and the Founding Director of Digital Futures. He has held visiting positions with UC Berkeley, Berkeley, CA, USA; Caltech, Pasadena, CA; NTU, Singapore; and other prestigious institutions. His research interests include networked control systems and cyber–physical systems with applications in transportation, energy, and automation networks.

Dr. Johansson was the recipient of numerous best paper awards and various distinctions from IEEE, IFAC, and other organizations for his scientific contributions. He was also the recipient of the Distinguished Professor by the Swedish Research Council, Wallenberg Scholar by the Knut and Alice Wallenberg Foundation, Future Research Leader by the Swedish Foundation for Strategic Research, and the triennial IFAC Young Author Prize and IEEE CSS Distinguished Lecturer, and the 2024 IEEE CSS Hendrik W. Bode Lecture Prize. His extensive service to the academic community includes being President of the European Control Association, IEEE CSS Vice President Diversity, Outreach and Development, and Member of IEEE CSS Board of Governors and IFAC Council. He has served on the editorial boards of *Automatica*, IEEE TRANSACTIONS ON AUTOMATIC CONTROL, IEEE TRANSACTIONS ON CONTROL OF NETWORK SYSTEMS, and many other journals. He has also been a Member of the Swedish Scientific Council for Natural Sciences and Engineering Sciences. He is Fellow of the Royal Swedish Academy of Engineering Sciences.